Discovering Monoterpene Catalysis Inside Nano-capsules with Multiscale Modeling and Experiments

Efrat Pahima,[a] Qi Zhang,[b] Konrad Tiefenbacher,[b,c] Dan T. Major [a,*]

[a] Department of Chemistry, Bar-Ilan University, Ramat-Gan 52900, Israel

[b] Department of Chemistry, University of Basel, Mattenstrasse 24a, 4058 Basel, Switzerland

[c] Department of Biosystems Science and Engineering, ETH Zurich, Mattenstrasse 24, 4058 Basel, Switzerland

ABSTRACT: Large-scale production of natural products, such as terpenes, presents a significant scientific and technological challenge. One promising approach to tackle this problem is chemical synthesis inside nano-capsules, although enzyme-like control of such chemistry has not yet been achieved. In order to better understand the complex chemistry inside nano-capsules, we design a multiscale nano-reactor simulation approach. The nano-reactor simulation protocol consists of hybrid quantum mechanics-molecular mechanics-based high temperature Langevin molecular dynamics simulations. Using this approach we model the tail-to-head formation of monoterpenes inside a resorcin[4]arene-based capsule (capsule *I*). We provide a rationale for the experimentally observed kinetics of monoterpene product formation and product distribution using capsule *I*, and we explain why additional stable monoterpenes, like camphene, are not observed. Based on the in-capsule *I* simulations, and mechanistic insights, we propose that feeding the capsule with pinene can yield camphene, and this proposal is verified experimentally. This suggests that the capsule may direct the dynamic reaction cascades by virtue of π-cation interactions.

Introduction

Terpenes are natural products derived biosynthetically from isoprene units. The basic molecular formula of terpenes is $(C_5H_8)_n$, where n is the number of isoprene units linked together in the form of linear chains or rings to form monoterpenes (n=2), sesquiterpenes (n=3), diterpenes (n=4), etc. Terpenes constitute one of the largest classes of natural products, and possess great structural diversity.[3-7] Terpenes also have a broad range of biological activities, such as antibacterial and anti-inflammatory activities,[8-10] and are used in treatment of human diseases, such as malaria[11] and cancer.[12-13] Terpenes also serve in the defense of many plants, animals and microorganisms against predators, pathogens and competitors,[6, 8-9, 14-15] and more.[5-6]

In nature, terpene chemistry follows a common mechanism, involving a sequence of electrophilic cyclizations, rearrangements, methyl transfers and H^+/H^- transfers via highly reactive carbocation intermediates. These intermediates must be guided in the correct reaction direction and protected from nucleophilic attacks and premature quenching, in order to minimize side product formation. This extremely challenging task is performed by terpene synthases (or cyclases), which are able to bind the acyclic terpene substrates in a product-like conformation, and guide the highly reactive carbocations towards the target product via specific electrostatic interactions.[7, 16-22] Additionally, terpene synthase reactions are driven by the inherent reactivity of carbocations.[23]

Terpene cyclases can be divided into two classes, which differ in the way the cationic cyclization cascade is initiated.[24-25] In class I terpene cyclases, an allylic cation is generated by heterolytic cleavage of a diphosphate leaving group with the help of divalent metal ions (e.g. Mg^{2+}), in a so-called Tail-to-Head Terpene (THT) cyclization.[7, 17, 22, 26-28] The activation at the tail end leads to the formation of a susceptible allylic cation, which is then chaperoned by the terpene cyclase towards the final product in a selective fashion.[7, 29] In solution, it has proven to be difficult to attain reaction specificity with THT synthesis, due to premature quenching by nucleophilic attack or elimination. Therefore, artificial catalysts able to perform selective THT cyclizations are lacking.[30-34] Class II terpene synthases utilize a Head-to-Tail Terpene (HTT) cyclization strategy,[35-36] where cyclization is initiated by direct protonation of a double bond or an epoxide. In contrast to THT, HTT chemistry has been intensively studied, and has been successfully reproduced in bulk solvent.[37-41]

Production of terpenes via bioengineering of metabolic pathways within microbial hosts like *E. coli* and *S. cerevisiae* were studied within the context of advanced biofuels synthesis.[28, 42-47] However, substantial yields were not obtained, although current research directions are constantly evolving and improving.[28, 46-53]
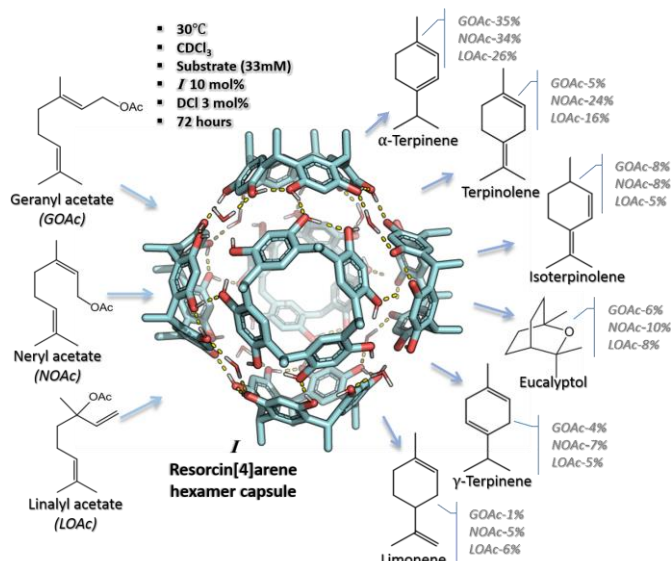
Figure 1. Partial summary of the experimental work of Tiefenbacher and co-workers.[1-2] Three different substrates (left) were fed into the resorcin[4]arene hexamer capsule in separate experiments, yielding various monoterpenes (right). Besides the formation of unidentified minor products, the rest of the substrate was consumed by alkylation of the phenols of the capsule and dimerization reactions.

Supramolecular capsules constitute an alternative to standard test-tube or microbial syntheses of terpenes. Molecular capsules provide means to mimic the basic working principles of the structurally complex natural enzymes by enabling the isolation of suitable substrates from bulk solvent in a hydrophobic cavity (i.e. the capsule). For example, in the resorcin[4]arene-based capsule (Fig. 1), the carbocation intermediates inherent to terpene chemistry are stabilized via cation-π interactions.[1-2, 29, 54-57] The importance of cation-π interactions[58] in nature were recognized by Kebarle and co-workers,[59] Diederich and co-workers,[60] Burley and Petsko,[61] and Dougherty and co-workers.[62] The interaction between cations (i.e. monopoles) and π-electron systems (i.e. quadrupoles) is considered to be largely electrostatic in nature.[58, 63-64] These interactions are ubiquitous in nature and are present in ion channels, receptors, enzymes, and more.[58] For instance, cation-π interactions have been found to be important in terpene synthases.[22, 65] Artificial systems that employ cation-π interactions are widespread, such as supramolecules in aqueous media, organic solvents and solid state.[58, 63, 66] A large variety of capsular host systems constructed from self-assembled monomers held together by metal–ligand interactions,[67-72] hydrogen bonds,[1, 73-75] or by hydrophobic effects[76] have been described in recent decades. The catalytic activity of host systems can stem from either the encapsulation of a chemically active species (e.g. a transition-metal catalyst) or the intrinsic properties of the cavity space (noncovalent interactions between host and guest, such as cation-π interactions).[77-80]

The resorcin[4]arene hexamer *I* (Fig. 1, 2) spontaneously forms in apolar solvents, like chloroform, from six resorcin[4]arene monomer units and eight water molecules. The capsule-like structure, held together by 60 hydrogen bonds, forms an octahedral-shaped cavity of about 1375 Å^3.[56] Due to extended cation–π interactions with the

aromatic cavity, positively charged intermediates, like carbocations in a THT mechanism, display high affinity for the capsule interior.[1-2] Besides the capability of reversible guest encapsulation, the resorcin[4]arene hexamer acts as relatively strong phenol-based Brønsted acid (pKa≈5.5–6).[81,82] Nevertheless, for many reactions, including terpene cyclizations, a Brønsted acid cocatalyst (e.g. HCl) is required.[83] Recent work of Tiefenbacher and co-workers focused on reactions using the precursors geranyl, linalyl and neryl, each with different leaving groups. By studying the influence of the leaving group on the product selectivity and product yield, as well as the relation of the leaving group affinity to the capsule walls, these authors managed to shed light on the mechanism of the reaction inside the capsule.[1-2, 84-85] However, each precursor and leaving group displayed different product distributions and reaction kinetics, and some resulted in low product yields.[1] Additionally, reaction specificity was not attained. Thus, a better understanding of the reaction mechanism inside capsule *I* is required, and the current study addresses this using multiscale modeling tools, which are augmented by in-capsule experiments.
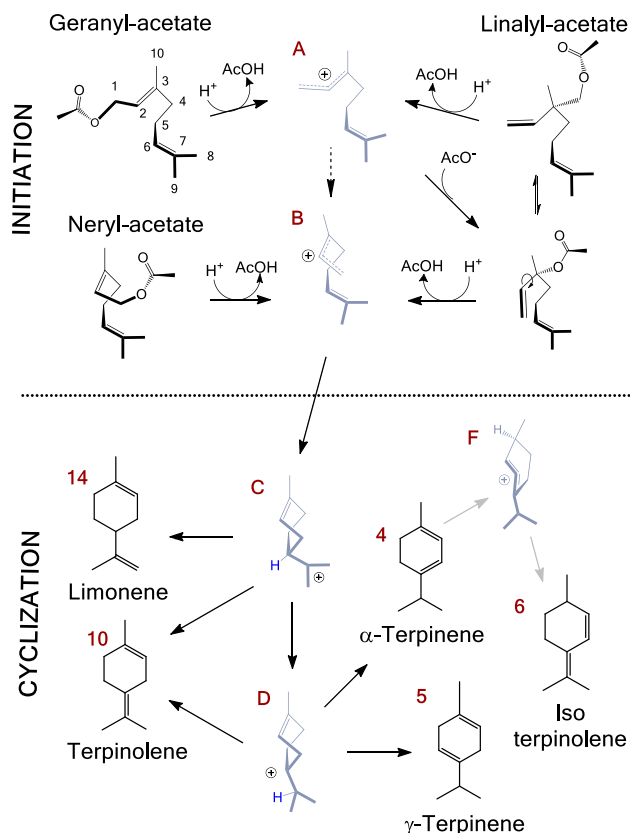
The primary goal of this study is to create a multiscale modeling protocol suitable for treating natural product synthesis inside a small nano-reactor (i.e. resorcinarene capsule *I*). We employ a hybrid quantum mechanics-molecular mechanics (QM/MM)[86] potential energy surface (PES) in conjunction with restrained high-temperature Langevin molecular dynamics (HT-LMD) simulations. The simulations target three substrates, geranyl acetate (GOAc), neryl acetate (NOAc) and linalyl acetate (LOAc), which have distinct product distribution profiles (Fig. 1).[1-2] Using this protocol, in addition to standard QM calculations, we obtain mechanistic insight into the many reactions occurring inside capsule *I*.

Computational Details

Gas-Phase Calculations. To gain in-depth understanding of the reaction mechanism occurring inside the resorcinarene capsule, it is important to understand the inherent energetics of the chemistry involved. Hence, density functional theory (DFT) gas phase calculations were performed, to shed light on stability, the possible reaction pathways and the energetic profiles of all products observed experimentally (Fig. 3, S2).

Prior to the DFT gas phase calculations, conformational searches were performed in order to determine the lowest energy conformers for each monoterpene, using Schrodinger's MacroModel[87-88] within the Maestro[89] modeling environment. Relative potential energies were determined using the OPLS3[90] force field.

Subsequent DFT geometry optimizations (minima and transition states, TS) and frequency calculations of the monoterpenes were performed in the gas phase using Gaussian 16, revision A.03[91] (see *Supporting Information* Scheme S1, Fig. S1 for all compounds included in the calculations). We employed the meta-hybrid GGA functional M06-2X, which has been shown to be accurate for thermochemical properties,[92-93] and also gives reliable results for carbocation chemistry relevant to terpenes.[18-19, 29] The basis set used was 6-31+G**.[94] Normal modes of vibration for the optimized molecules were inspected to verify the nature of the stationary points. To confirm that a given TS connects

2

Scheme 1. Reaction mechanism for geranyl, neryl and linalyl acetate inside the resorcinarene capsule. The black arrows represent the mechanism suggested by Tiefenbacher and co-workers.[1-2] Other possible reaction mechanisms are presented in Fig. 5 and Scheme S1.

between reactant and product wells, we performed intrinsic reaction coordinate (IRC) calculations.[88, 95] The free energy profiles reported herein were computed using electronic energy combined with zero-point energy and thermal corrections, using statistical mechanics expressions within the harmonic approximation.[96] Entropy errors resulting from not treating free rotations explicitly are ~0.5 kcal/mol per freely rotatable bond (at room temperature), and may be ignored for this study.[97]

Possible reactions occurring inside the resorcinarene capsule are summarized in Scheme **1**.

Resorcinarene Capsule Modeling. The initial coordinates for the capsule simulations were obtained from the crystal structure of the resorcinarene capsule **I** (Fig. 1).[56] All calculations were performed with methyl groups replacing the R=$C_{11}H_{23}$ chains. The complete capsule **I** nano-reactor system includes the following (Fig. 2): The resorcinarene capsule, composed of six resorcinarene monomer units and 8 water molecules, one HCl molecule (acid catalyst), 5 or 6 chloroform solvent molecules (further details below), and a substrate (either GOAc, NOAc, or LOAc). The resorcinarene capsule, water, and solvent molecules were treated with MM. Force field parameters and residue topology were developed based on existing CHARMM FF C22 and C36 parameters.[89, 98-105] Water molecules were treated by the TIP3P model.[106] Chloroform parameters were adopted from CHARMM general FF (CGenFF[89]) and the SHAKE algorithm was employed to constrain the solvent geometry.[107] All parameters and residue topology files can be found in
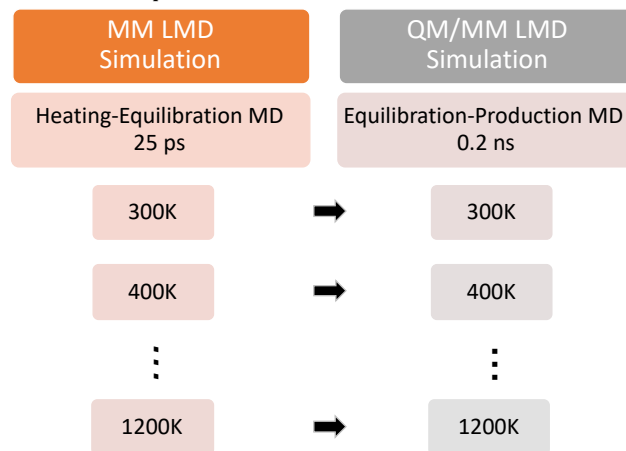
the Supporting Information. Most simulations were performed for each substrate in both 5 and 6 solvent molecules capsule **I** systems, since it is unknown how many solvent molecules occupy the capsule when the substrate is present. Indeed, we assume both scenarios are plausible.

QM/MM In-Capsule Chemical Modeling. The substrate (either GOAc, NOAc, or LOAc), and in some cases also HCl, were treated using the M06-2X functional, with the following basis set combination: the carbon and hydrogen atoms were treated with the 6-31G* basis set, the oxygen and chlorine atoms were treated with 6-31+G*. The interactions between the QM and MM regions were treated using electrostatic embedding. No cutoff values were employed in computing the MM or QM/MM interactions.

All simulations in the capsule system were performed using a QM/MM scheme that combines the CHARMM program[103-104] and Q-Chem.[108]

QM/MM Nano-Reactor Simulations Protocol Overview. The simulations performed on capsule **I** include minimization and LMD heating, equilibration and production simulations, with nano-reactor simulation protocol settings mimicking the experimental conditions (see similar nano-reactor simulations in Ref. [109]). The experiments of Tiefenbacher and co-workers were performed at 30 °C in CDCl₃, with a substrate concentration of 33.3 mM, 3 mol% DCl and 10 mol% capsule. The results were collected over a 72 hours period of time.[1-2] With today's computational resources, such long LMD QM/MM simulations are not realistic, as they are too expensive. In order to observe reactive events occurring in reasonably short simulation times, we employed a HT-LMD strategy. The simulations commenced by slowly heating the system from 300K to 1200K using a MM PES. Formally, the temperature for our LMD simulations may be defined as 300+(100·n) K, with n running from 0 to 9. In practice, we raised the temperature by 100K every 25 ps simulation time, resulting in an overall simulation time of 0.25 nano seconds. Restraints were added to the capsule to keep it intact at elevated temperatures (further explanation about these restraints are presented in the following section and in the *Supporting Information*).

Chart 1. Illustration of the QM/MM nano-reactor simulations protocol.

Following this heating period, we switched to a QM/MM PES. Each temperature step (i.e. 300K, 400K, …, 1200K) was further simulated using QM/MM LMD, starting
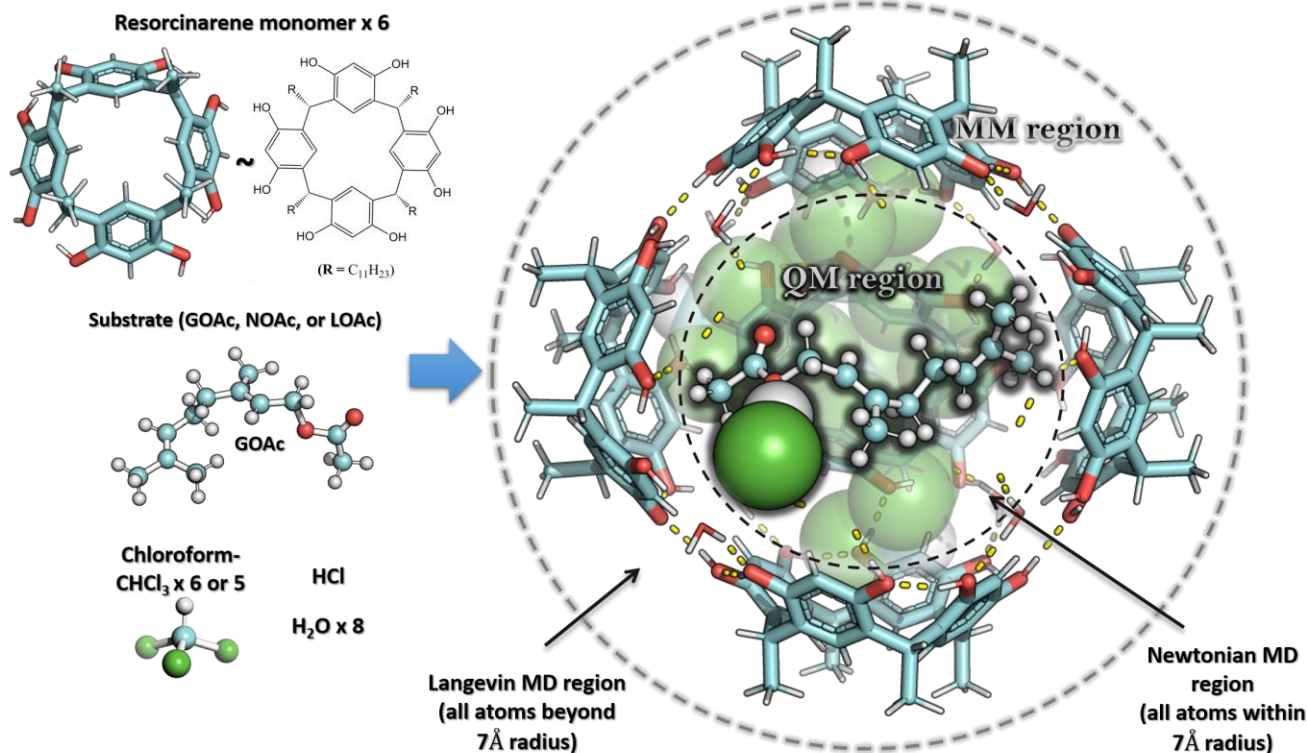
3

Figure 2. *In silico* capsule *I* system. The hexameric resorcinarene capsule *I* is composed of six resorcinarene monomers and eight water molecules, held together via hydrogen bonding in apolar solvent. The capsule is capable of stabilizing cationic guests inside its cavity via cation–π interactions.[1-2] The capsule includes the chloroform solvent, one pair of H^{+} and Cl^{-} ions and the substrate (either GOAc, NOAc or LOAc). The QM region is highlighted with black shading (the substrate, Cl^{-} ion, and proton), while all other residues belong to the MM region. Atoms in the outer Langevin region are propagated via Langevin's equations, while atoms in the inner region are treated by Newton equations of motion.

from the MM heating restart conditions. The simulation time for each QM/MM LMD simulation was 0.2 ns. At each temperature, we performed two simulations for each substrate, using 5 or 6 solvent molecules. It was expected that chemical reactions would occur at elevated temperatures, where the system has sufficient kinetic energy to cross activation barriers, in spite of the short simulation times. This intuitive expectation is based on the known high reactivity of carbocations. Further details about these simulations are illustrated in Chart 1 and explained in the following section.

QM/MM Nano-Reactor Simulation Protocol Details. The equations of motion were integrated numerically using Langevin dynamics. The Langevin equation was employed for all atoms beyond 7 Å of the origin (center of capsule). In practice, this means that all capsule *I* atoms (but not solvent, HCl, or substrate) feel a friction force (with a friction coefficient of 7 ps[-1]) and also experience an occasional random "kick" to maintain the desired target temperature during the simulation. The atoms inside the capsule (within 7 Å) are thermostatted via stochastic collisions with the capsule atoms. Thus, the Langevin atoms (i.e. capsule atoms), are subjected to NVT dynamics (constant particle-volume-temperature), while the inner atoms (solvent, HCl, and terpene) are formally under NVE conditions (constant particle-volume-energy) dynamics. However, in practice the inner atoms are subjected to NVT dynamics by virtue of their collisions with the capsule.

The thermal motion rapidly breaks apart non-covalent interactions at high temperatures, thus the capsule itself must have restraints so as to not break apart. Nuclear Overhauser effect (NOE) restraints were applied to the capsule's hydrogen bonds to assure that the capsule will not disintegrate during the HT-LMD. The simulations employed the Leap-Frog integration scheme with a time step of 1 fs.[107]

Experimental Details

Transformation of ß–pinene catalyzed by the resorcinarene capsule *I*. *Procedure for the cyclization reaction.* Chloroform was filtered through basic aluminum oxide prior to usage. To a solution of the resorcinarene capsule *I* (11.1 mg, 1.67 µmol, 0.10 eq) in chloroform (200 µL) were added successively HCl stock solution in chloroform (0.50 µmol, 0.03 eq) and *n*-decane stock solution in chloroform (20 µL, 167 mmol/L, 3.34 µmol, 0.2 eq). Then additional chloroform was added to reach a total volume of 500 µL for the reaction mixture. After β–pinene (2.63 µmol, 16.7 µmol, 1.00 eq) was added, the reaction mixture was briefly agitated. An aliquot (approx. 10 µL) of the reaction mixture was diluted with 0.2 mL *n*-hexane and subjected to GC analysis (initial sample). Meanwhile, the reaction was kept at the given temperature (30 °C, 40 °C and 50 °C, respectively). After the indicated time, the reactions were sampled as described above. Cyclization products were identified by comparing the NMR and GC spectra of the reaction mixtures with those of the authentic monoterpene samples. Conversions and yields were calculated as described in Ref. [2]. For the preparation of resorcinarene capsule *I* and HCl stock solution, see Ref. [110].

4

1	2	3	4	5	6	7	8	9	10	11
0.0	0.9	1.0	1.9	2.8	3.1	3.5	3.5	3.9	4.6	5.5
		α-Camphene	α-Terpinene	γ-Terpinene	Isoterpinolene		β-Camphene	α-Fenchene	Terpinolene	γ-Mendatiene

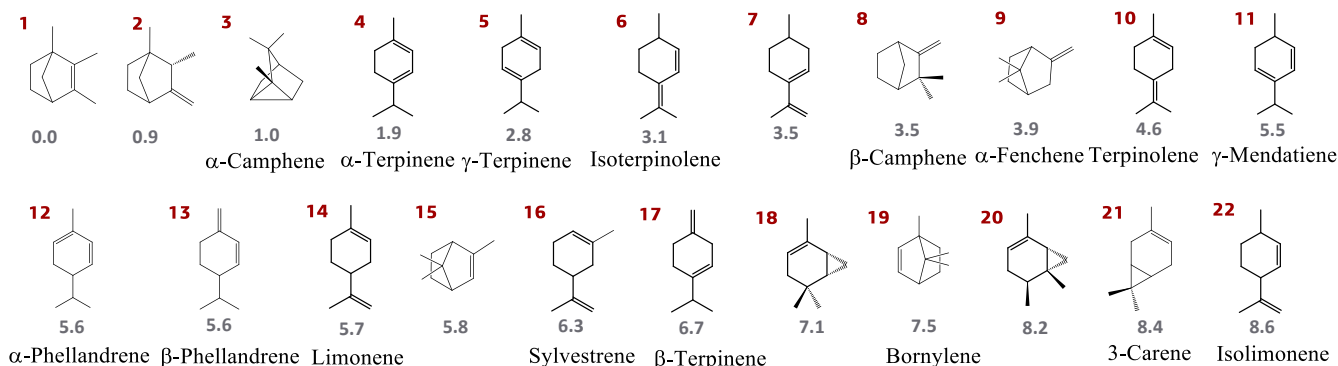| 12	13	14	15	16	17	18	19	20	21	22
5.6	5.6	5.7	5.8	6.3	6.7	7.1	7.5	8.2	8.4	8.6
α-Phellandrene	β-Phellandrene	Limonene		Sylvestrene	β-Terpinene		Bornylene		3-Carene	Isolimonene

Figure 3. Relative free energies (kcal/mol) of monoterpenes, including the products observed in the experimental work of Tiefenbacher and co-workers (see Fig. 1), potential products that can result from the carbocations observed in the current QM/MM HT-LMD simulations, and additional monoterpenes. The calculations were performed at the M06-2X/6-31+G** level of theory. The complete figure, consisting of 52 monoterpenes can be found in the SI (Fig. S2).

Results

The following section is divided into three parts: (1) Extensive DFT study of the free energy of monoterpenes (the experimentally observed products in capsule *I* and other known monoterpenes) in the gas-phase; (2) QM/MM HT-LMD simulations, mimicking the carbocation chemistry occurring inside the resorcinarene capsule; (3) Further gas-phase calculations of the carbocation intermediates observed in the HT-LMD simulations.

(1) Thermodynamics of monoterpenes. In order to understand the inherent energetics of the chemistry involved we performed DFT gas-phase calculations at the M06-2X/6-31+G** level. The question guiding us in this part is to what extent the experimental product distribution observed from capsule *I* synthesis is dictated by the intrinsic thermodynamics of monoterpenes.

Fig. 3 and S2 compare the relative computed free energies of an assortment of known monoterpenes (**1-22**), as well as novel monoterpenes generated by using some of the carbocation structures found in the study of Jacobson et al.[111] The monoterpenes predicted to be most stable are **1**, **2** (fenchyl-cation derivatives) and α- and β-camphene (bornyl cation derivatives), followed by experimentally observed α- and γ-terpinene, and additional monoterpenes that possess a terpinyl carbon skeleton (< ~5 kcal/mol of global minimum). Seemingly the relative stability of the monoterpenes is a combination of the number and nature of chemical bonds (σ, π, conjugated), ring strain, and steric crowding.

This computed monoterpene free energy landscape may be compared with the products observed experimentally via in-capsule *I* synthesis.[1-2] The in-capsule *I* synthesis yielded the following main monoterpene products: α-terpinene, terpinolene, isoterpinolene, γ-terpinene, and limonene (Fig. 1). Hence, the observed monoterpenes are all within a few kcal/mol of the global monoterpene minimum. The computed order of stability is α-terpinene (most stable) > γ-terpinene > isoterpinolene > terpinolene > limonene, while experimentally the order is (using NOAc as substrate) α-terpinene > terpinolene > isoterpinolene > γ-terpinene > limonene. We note that the experimental data reported here are those after 72 hours, at which time the products had not yet reached a plateau. Indeed, at 72 hours the amounts of α-terpinene, γ-terpinene, and isoterpinolene

were increasing, while the amounts of terpinolene and limonene were decreasing. In particular, the amount of terpinolene was decreasing sharply. Hence, the product distribution seems to be moving towards the thermodynamic partitioning. To validate the accuracy of our DFT approach, we also compared the relative stability of all monoterpenes using the highly accurate CBS-QB3 and G4 methods.[112-114] These results confirm the general trends predicted by DFT (Table S4). We may therefore conclude that the in-capsule *I* synthesis preferably produces low-energy monoterpenes. However, important questions do remain unanswered, namely how come additional low-energy monoterpenes such as α- and β-camphene are not observed experimentally? Under what conditions can they form in the capsule? Additionally, what role does the initial substrate play in the experimental product distribution? To answer these questions, we performed in-capsule *I* simulations.

(2) In-capsule *I* HT-LMD QM/MM Simulations. As explained in the *Computational Details* section, the interactions in the capsule/substrate/chloroform system are treated via a hybrid QM/MM potential, while the dynamics of the system is treated via HT-LMD simulations. For all systems, the room temperature simulations did not produce chemical events during short trial simulations, and below 500K not many reactions occurred (not shown). Hence, our discussion will focus on the HT simulations. Fig. 4,a-c presents the intermediates observed during the simulations performed at a range of temperatures from 500K to 1200K. The results are for three substrates, GOAc, NOAc, and LOAc, and the systems include 6 chloroform molecules. Results for identical systems, but with 5 chloroform molecules, are presented in Fig. S3,a-c.

As expected, the number of chemical events greatly increases with temperature. Beyond ~1100-1200 K, we observe higher energy chemistry that includes fragmentation of the carbocation skeleton structure (which rearranges back to yield different carbon frameworks) and creation of carbanions. Seemingly, the optimal temperature for these monoterpene HT-LMD simulations is ~900K-1000K. For the purpose of the discussion below, we will treat all HT simulations (T ≥ 500K) with 5 or 6 chloroform solvent molecules as an ensemble of trajectories that reflect what occurs during experiments. Due to the limited simulation time, the diverse product distributions obtained during the various simulations (different temperatures and number of
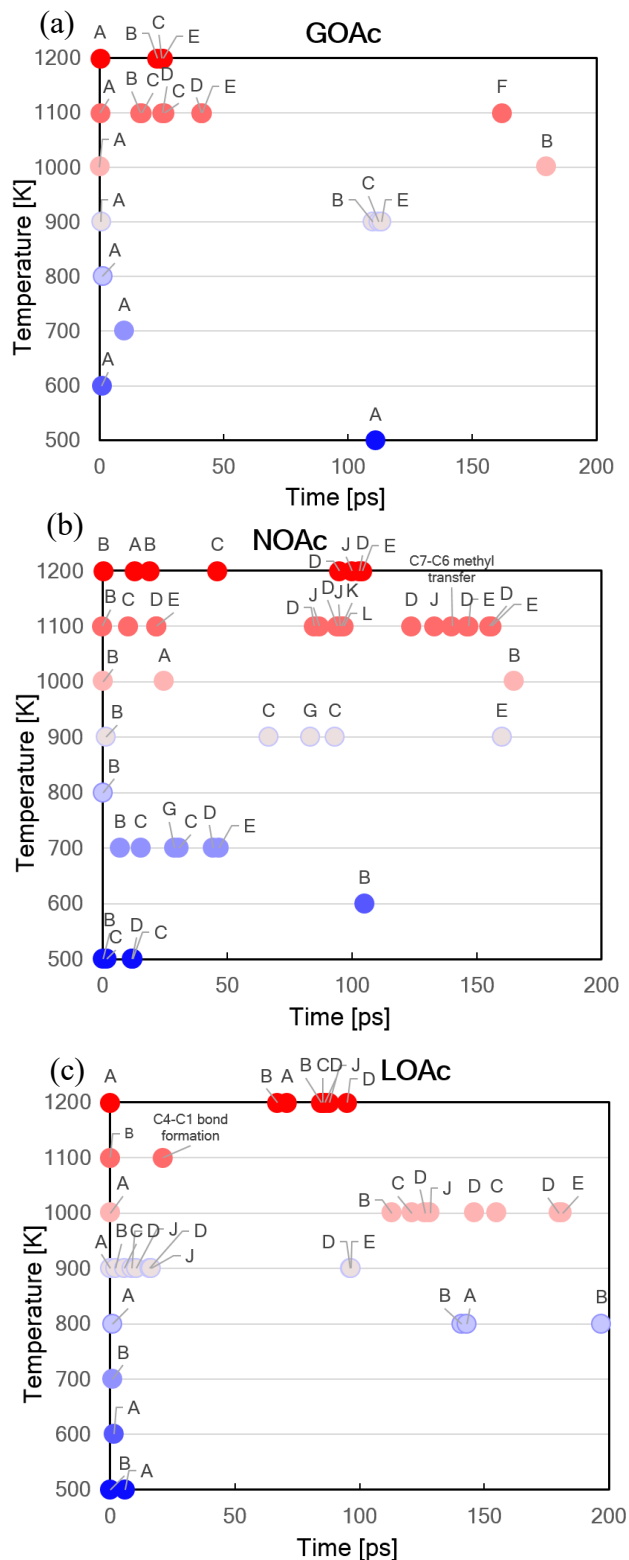
solvent molecules) do not necessarily reflect meaningful statistical differences between the *in-silico* simulation conditions. Yet, inspection of the global carbocation pool observed during all simulations, can provide qualitative insight into what occurs in a wet-lab setting.

The in-capsule *I* reactions commence with protonation of the ester oxygen of GOAc, NOAc, and LOAc. Initial C-O heterolytic bond dissociation takes places within the first few ps of the simulations for all T ≥ 500K. This first step results in an allyl cation, which in the case of NOAc is in a reaction-ready Z-conformation **B**, while for GOAc is in a non-reactive E-conformation **A** (Scheme 1). In the case of LOAc, the allyl cation conformation obtained depends on the conformation around the C2-C3 bond at the time of C-O bond cleavage. These differences in the substrates in capsule *I* are reflected in the time required for initial cyclization to form the first intermediate α-terpinyl cation, **C** (Fig. 4,a-c). In GOAc, the first instance of **C** formation was observed at 900K, while for NOAc, we observed its formation already in the simulation at 500K. In the case of LOAc, we observe **C** formation at 900K. Interestingly, we observe that the reaction-ready cation **B** has a distinct life-time of several psec, which suggests that formation of cation **C** from the initial substrate is only a partially concerted process. This is in contrast to what has been suggested based on experiments,[1] but is in line with what we have observed in numerous simulations for class I terpene synthases.[18-21, 29, 115-117] On the other hand, the GOAc reaction is distinctly step-wise.

Once cation **C** is formed, a rich assortment of reactions may take place (Scheme 1, Figures 4,a-c, 5). Direct deprotonation of **C** would give limonene or γ-terpinene (deprotonations not modeled, as capsule atoms are defined as MM). A 1,2-hydride transfer gives terpinene-4-yl cation, **D**, which upon deprotonation would produce α-terpinene, γ-terpinene, or terpinolene (Scheme 1). A subsequent 1,2-hydride transfer produces the allylic terpinene-3-yl cation **E** (**E** can also form via a 1,3-hydride shift from **C**). Deprotonation of **E** would yield α-terpinene or α- or β-phellandrene. Additional hydride shifts are possible,[18-19, 29, 118-121] but were not observed in our short simulations. The direct carbocation precursor to isoterpinolene can be formed by a 1,5-hydride transfer or deprotonation/reprotonation mechanism from cation **E**, and in our simulations was formed via deprotonation/reprotonation by carboxylic acid.

Cation **C** also underwent electrophilic attack by the C2-C3 double bond to form a pinyl cation, **G**, which rearranged to give a bornyl cation, **H** (but not cation **M**, see Fig. S3,a-c, S4). Cation **H** immediately rearranged to yield a tertiary camphyl cation, **I**. **G** can give the high energy monoterpenes α- and β-pinene, **H** can result in bornene or further rearrange to yield α-camphene, while **I** can result in β-camphene. These results suggest that a variety of terpene products potentially could form in the capsule. However, many products were not observed experimentally,[1-2] and we will discuss the reason for this below.

Cation **D** may also undergo electrophilic addition to give sabinyl cation **J**, which could be deprotonated to give sabinene or α-thujene. Methylene rearrangement results in **K**, and a propyl ring opening of **K** can give an additional terpinyl cation **L**, which can give α-, β-, or γ-terpinene upon deprotonation.

Figures 4,a-c. Heat maps representing the monoterpene intermediates observed in the QM/MM HT-LMD simulations of capsule *I* over the course of 0.2 ns for temperatures 500K-1200K. The capsule *I* system had 6 chloroform solvent molecules. Starting materials were (a) GOAc, (b) NOAc, and (c) LOAc. Labels (A-O) refer to cationic intermediates (see Fig. 5).

6

Hence, a variety of carbocations (**A-L**) are formed during our HT-LMD simulations, suggesting that not only the experimentally observed monoterpenes can form via their carbocation precursors **C-F**, but also other monoterpenes such as the α, β-camphene, α, β-phellandrene, sabinene and α, β-pinene. Importantly, carbocation precursors for all products observed from in-capsule **I** experiments (i.e. α-terpinene, terpinolene, isoterpinolene, γ-terpinene, and limonene) are seen in our QM/MM HT-LMD simulations, and this is a key finding of this study.

Now we turn back to a question left unanswered from the previous part. We see various intermediate precursors to other potential low energy products in our simulations, posing the question how come α, or β−camphene, or phellandrene are not observed in the experimental

work? For this reason, we return to DFT gas phase calculations of the detailed mechanism to study the carbocation chemistry observed in the HT-LMD simulations.

(3) Free Energy Profiles for Monoterpene Formation. The current approach allows a peek into the real-time dynamics of the terpene chemistry occurring inside capsule **I**. However, the simulations aren't sufficiently long to explain the detailed product distribution. Indeed, to explain the experimentally observed product distribution would require either very long simulations, or a swarm of parallel simulations to collect significant statistics for the observed chemical events. In order to gain quantitative insight into the thermodynamic details of the product distribution, we turn to mechanistic DFT calculations along predefined reaction paths that lead to products suggested by Tiefenbacher and co-workers and as seen in our HT-LMD
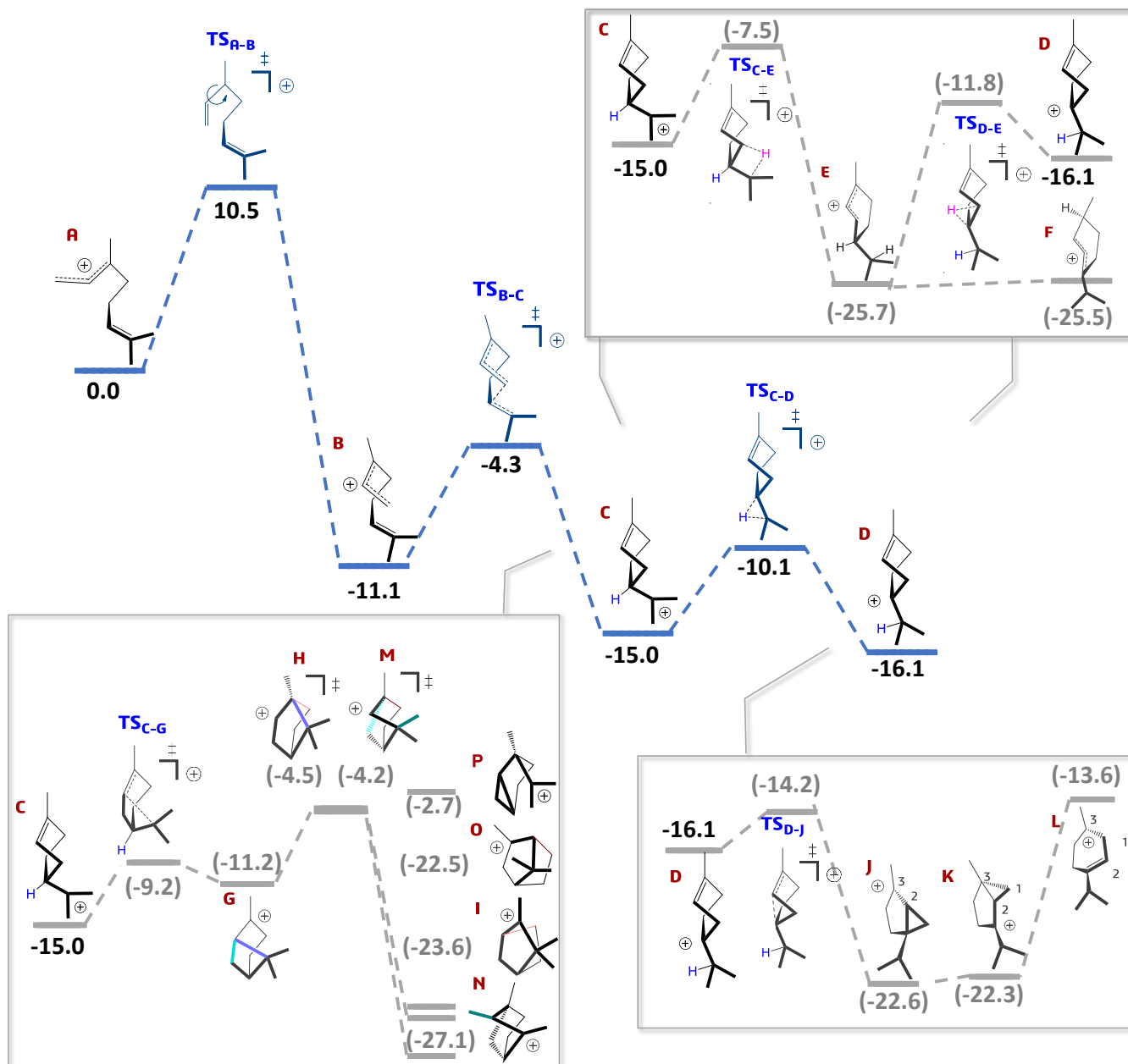

Figure 5. Free energy profile (kcal/mol) for a model reaction for the monoterpene pathway, starting from (**A**) 2,3 transoid-cation. Blue curves represent the mechanism suggested by Tiefenbacher and co-workers,[1-2] grey lines represent alternative mechanisms observed in our QM/MM HT-LMD simulations and intermediates that were less favorable energetically. The calculations were performed at the M06-2X/6-31+G** level of theory.

simulations. We note that this analysis is similar to our previous work on monoterpenes and that of Hong and Tantillo.[18, 121]

In principle, we could compute the free energy barriers inside the capsule, using techniques such as potential of mean force, but such simulations are rather expensive. In the current case, we presume it is sufficient to model the reactions in gas-phase, as the effect of the capsule is expected to be similar for all reaction paths. As will be discussed below, this assumption might not hold for all cases.

As shown in Fig. 5, the transoid **A** to cisoid **B** linalyl cation direct rotational transition suggested by Tiefenbacher et al. has a relatively high free energy barrier of 10.5 kcal/mol. However, this rotational barrier can be significantly reduced if cation **A** is partially recaptured by acetic acid. Indeed, this is the strategy adopted in class I terpene cyclases.[122-124] Inspection of Fig. S1 and Scheme S1, the transition going through **LOAc** has lower activation free energies (**A** to **LOAc** and **LOAc** to **B** have activation free energies of 1.0 kcal/mol and 4.9 kcal/mol, respectively). However, both direct and acetic acid-assisted pathways were observed in the QM/MM HT-LMD simulations.

B is more stable than **A** by 11.1 kcal/mol, which may be due to the folded structure of **B**, with a short C1 and C6 distance (1.65 Å). This state of **B** resembles the α-terpinyl cation, **C**, (C1-C6 bond length: 1.53 Å), but with the positive charge resonating between the C1-C2-C3 carbons and the C6-C7 π-system. Following generation of **B**, terpinyl cation **C** is readily produced via C1-C6 bond formation (-15.0 kcal/mol). The following **C** to **D** 1,2-hydride shift has a 4.9 kcal/mol activation free energy. **C** and **D** are nearly isoergonic (reaction free energy of -1.1 kcal/mol), as both consist of a similar tertiary carbocation. Based on our QM/MM HT-LMD simulations, we discovered an additional plausible pathway from **C** to **D**, going through the stable allylic carbocation terpinen-3-yl-cation, **E**, with a -10.7

kcal/mol reaction energy for the **C** to **E** reaction and an activation free energy of 7.5 kcal/mol. The subsequent transition from **E** to **D** is endergonic (free energy barrier of 13.9 kcal/mol and reaction free energy of 9.6 kcal/mol). However, the **E** carbocation can also lead to α-terpinene, which is the most abundant product in Tiefenbacher and co-worker's experiments.[1-2] Considering the lower barrier of the **C**→**D** transformation, this is the more likely pathway.

Pinyl cation, **G**, results from **C** via TS$_{C-G}$, with a free energy barrier of 5.8 kcal/mol, which is slightly higher than the **C**→**D** transition, and with an endergonic reaction free energy of 3.8 kcal/mol. Deprotonation of cation **G** can lead to the α- or β-pinene product. Earlier work has shown that bornyl cation, **H**, is a high-energy secondary carbocation (transition state).[19, 121] Here we compute the activation free energy for the **G**→**H** transition to be 6.7 kcal/mol (Fig. 5, 6). Similarly, fenchyl cation, **M**, which has also been shown to be a first-order saddle point,[19, 121] can form from **G** with a similar activation free energy (7.0 kcal/mol). Interestingly, both **H** and **M** have been shown to be bifurcation points,[19] and can branch in the directions of camphyl (**I**) and **P**, and cations **N** and **O**, respectively.[18, 29, 115, 118, 121] Camphyl cation is a precursor for monoterpenes α- and β-camphene, while fenchyl cation is a precursor for α- and β-fenchene (Fig. 3). Additionally, bornyl cation **H** can form the high-energy cation **P** (precursor for **41**),[19] while fenchyl cation **M** can form low-energy cation **N** (pre-cursor for **1** and **2**). Our earlier gas-phase work[18] suggested that both bornyl **H** and fenchyl **M** cations should be formed with equal probability in the absence of a capsule, suggesting we should observe low-energy cations **I**, **N**, and **O** in our HT-LMD simulations. We do observe camphyl cation, **I**, (and the preceding bornyl cation, **H**), but do not observe fenchyl cation, **M**, or **N** and **O** in our HT-LMD simulations. In order to test these assumptions, i.e. **H** and **M** should form with equal probability, we performed further QM/MM HT-LMD simulations (Fig. S4). By using the initial 900K restart conditions for pinyl cation, we implemented an algorithm for changing the momenta of all atoms in the simulation via random kicks, similar to transition path sampling.[125] Hence, we sampled additional regions of phase space in the vicinity of pinyl cation in an attempt to observe fenchyl cation **M**. The results are presented in Figure S4, and show that no fenchyl cation was observed.

Additionally, we calculated the average distance of the following carbocations from the capsule's walls: pinyl, **G**, camphyl, **I**, α-terpinyl, **C**, bornyl, **H** and fenchyl, **M**. All distances were measured from the charged carbon to the nearest resorcinarene monomer. Specifically, the distances were defined from the cation to the three carbon atoms of the four phenyl rings, connected to the OH groups (named CZ1, CZ2, CD2 in the SI rtf files). See Fig. 7a,b and SI Table S5 and Fig S6 for further details. We found that pinyl cation **G**'s C3 position is 5.4 Å (±0.8 Å), camphyl **I**'s C3 is 5.8 Å (±0.7 Å) and α-terpinyl cation **C** C7 is 5.4 Å (±1.0 Å) from the capsule's walls. To probe the distance between the secondary carbocations bornyl, **H**, and fenchyl, **M**, and the capsule wall, special distance restraints were imposed on the bonds to avoid rearrangement (further information can be found in the SI). Analysis of the MD trajectories revealed that the bornyl C2 ensemble averaged distance from the capsule
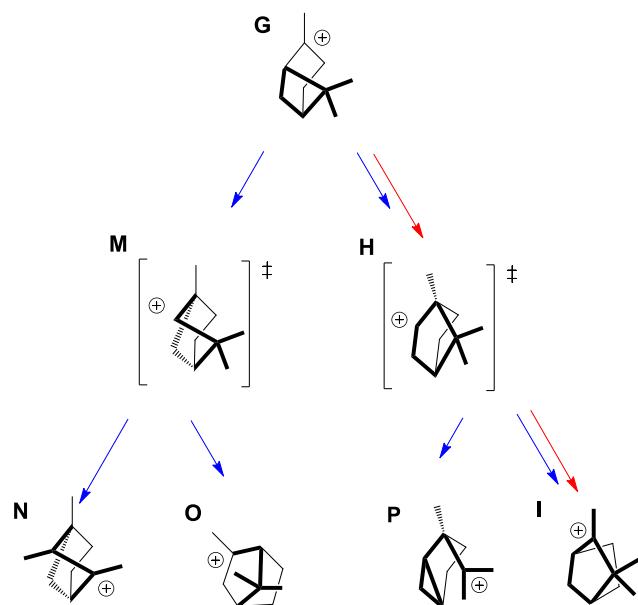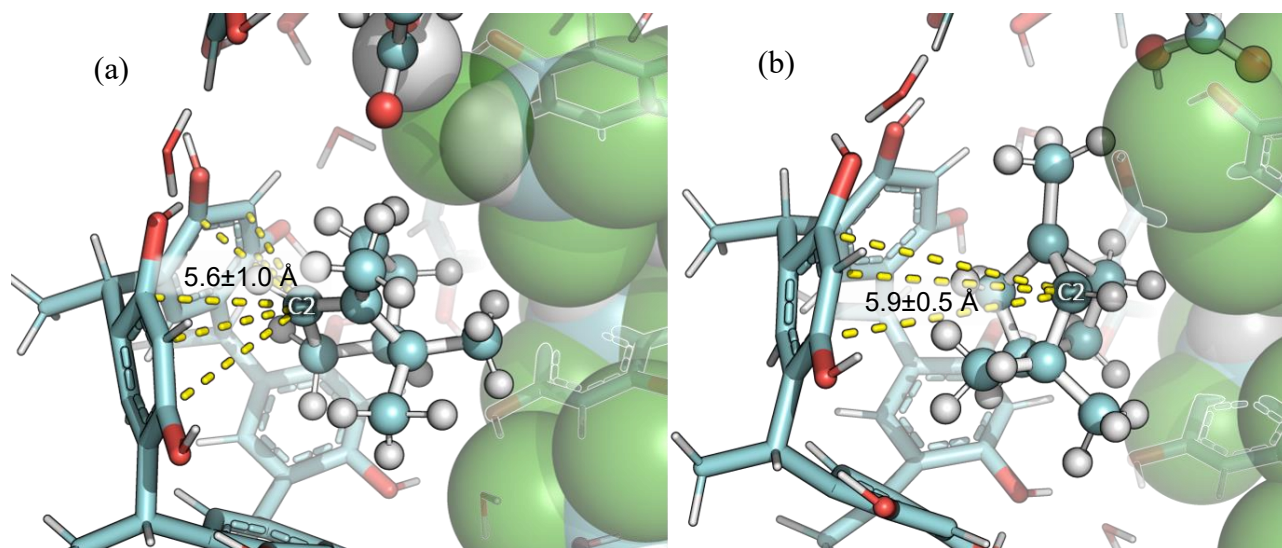

Figure 6. Possible carbocation pathways in the gas-phase (blue arrows) and in capsule *I* (red arrows). Length of arrows correspond to probability of step (see kinetic and thermodynamic data in Figure 5).

Figures 7a,b. Cation-π interactions between monoterpene carbocations and capsule *I*. The left figure (a) shows bornyl cation, **I**, and the right figure (b) shows fenchyl cation, **M**.

wall is 5.6 Å (±1.0 Å), and the fenchyl C2 distance from the wall is 5.9 Å (±0.5 Å) (Fig. 7a,b). We ascribe this difference to the greater steric hindrance in fenchyl cation, due to the additional bulky propylene group in the position adjacent to the cation. Hence, we conclude that an unhindered secondary carbenium, **H**, may be preferentially stabilized by capsule *I*. Since both bornyl and fenchyl cations are bifurcation points, we consider this capsule *I* stabilization of the bornyl pathway a dynamic effect.

To probe whether these in silico observations are reproducible in the lab, we performed in-capsule *I* experiments by feeding the capsule with β–pinene (precursor for cation **G**, see Fig. 6). The rationale for using β–pinene as a starting material is that the effective barrier to camphene formation is smaller than when starting from a linear precursor. In this case, we observe formation of significant amounts of camphene, yet no fenchene was formed (Table 1, Fig. S5). We also observe formation of limonene, terpinolene, α- and γ-terpinene, which are a result of the ring-opening of pinyl cation, **G**, to terpinyl cation, **C**. Hence, there is full agreement between experiments and theory. We speculate that the interaction between the capsule π-system and the secondary cation carbon in bornyl, **H**, is stronger than for fenchyl cation, **M**, due to greater steric hindrance in

proximity of the cation in the latter. This is supported by the ensembled averaged distanced presented above. Hence, bornyl cation may be preferentially stabilized by the walls of the capsule. This suggests that the capsule can direct the dynamic reaction cascade in the direction **G→H**, away from **G→M**, by virtue of π-cation interactions. We have previously shown that the enzyme bornyl diphosphate synthase can similarly modulate bifurcation behavior in monoterpene systems.[19]

Sabinyl cation, **J**, results from **D** via TS$_{D-J}$, with a 1.9 kcal/mol activation barrier and an exergonic reaction free energy (-6.5 kcal/mol), and can lead to sabinene or α-thujene. Carbocation **K** is formed by a methylene transfer from C6 to C3, and might proceed to cation **L** via an endergonic reaction (8.7 kcal/mol), which can lead to various terpinenes. Although cations **J** and **K** are relatively stable, the corresponding monoterpenes (sabinene, α-thujene, **25**, **27**) are not (Fig. 3), and thus these are not observed experimentally although their carbocation precursors may exist in capsule *I*.

Table 1: Experimental data for the capsule I-catalyzed conversion of β-pinene as substrate (standard reaction conditons, for more information see SI). The reaction was performed at three different temperatures (30-50 °C).

T	Conversion[a]	limonene[b]	camphene[b]	terpinolene[b]	α-terpinene[b]	γ-terpinene[b]
30 °C	19%	5%	2%	1%	1%	0%
40 °C	72%	24%	12%	5%	3%	1%
50 °C	99%	33%	18%	9%	5%	2%

[a] Conversion after 41h, quantified by gas chromatography; [b] Yields of products after 41h; products were identified by gas chromatography and ^{1}H NMR spectroscopy and quantified by gas chromatography.

Discussion

In this section we will discuss two important questions relating to natural product synthesis inside nano capsules:

1. Observed product distribution. Specifically, what dictates the product selectivity inside capsule *I*?

2. Influence of substrate. Specifically, can we explain the difference in the product distribution between the substrates geranyl, neryl and linalyl acetate?

First, we tackle the product selectivity question. Specifically, are the experimentally observed monoterpenes also the lowest energy ones? For this reason, we performed DFT M06-2X gas phase calculations for an assortment of monoterpenes (Fig. 3, S2). We found that the in-capsule *I* observed monoterpenes are all within a few kcal/mol of the global monoterpene minimum. The monoterpene product with the highest experimentally observed yield is α-terpinene, **4**, which may be explained by **4** being the monoterpene with the lowest free energy among the different products observed experimentally.[1-2] Limonene, **14**, has the highest free energy among the experimentally observed products, and thus has a very low experimental yield. High-level CBS-QB3 and G4 ab-initio calculations corroborate these DFT results. However, low energy monoterpenes, such as products **1**, **2**, α and β-camphene and α and β-phellandrene were not observed experimentally. This inspired us to perform QM/MM HT-LMD simulations in an attempt to observe the chemistry as it takes place inside the capsule.

The simulations showed that a broad spectrum of monoterpene products can form inside the resorcinarene capsule, via carbocation chemistry. Additionally, the data suggests that when provided with sufficient kinetic energy, such as in our HT-LMD simulations, kinetically disfavored pathways to thermodynamically preferred monoterpenes are attainable. For instance, camphyl cation, **I**, en route to camphene, was observed. This suggests that the designed HT-LMD simulation protocol can readily describe the different types of carbocation chemistry occurring inside nano-capsules. However, camphene was not observed experimentally and to answer this we turned to detailed DFT gas-phase studies of the mechanistic possibilities suggested by Tiefenbacher and co-workers and by our HT-LMD simulations.

As shown in Fig. 5, camphenes are obtained via pinyl cation, **G**. The TS forming **G** from **C,** TS$_{C-G}$, is slightly higher in free energy (by 0.9 kcal/mol) than the competing pathway TS$_{C-D}$, which forms terpinene-4-yl-cation, **D**. Hence there is a slight kinetic preference for the latter pathway. Additionally, the pinyl to bornyl pathway, **G→H**, has a free energy barrier of 7 kcal/mol, and the combined barrier from **C→H** is 10.8 kcal/mol. Similarly, the barrier for **C→E** is significantly higher than **C→D** (7.5 kcal/mol), explaining why phellandrene isn't observed. This indicates a strong kinetic preference for **C** and **D**, and therefore for all the subsequent deprotonation species that are observed experimentally.

Thus, for the first question we can answer that the selectivity of the products is dictated by a balance of thermodynamic and kinetic control: the experimentally observed products are low-energy species with low-energy carbocation precursors; and the height of the free energy barriers dictates which pathways are accessible. This proposal is further supported by in-capsule *I* experiments starting with β-pinene, which yielded camphene as a main product. It seems that the interaction between the capsule π-system and the secondary cation **H** favors this pathway over the pathway via **M** (Fig. 6).

In order to tackle the second question, regarding the difference in product selectivity for the different substrates, we focus on a specific case; namely the difference in formation of α-terpinene and terpinolene using GOAc and NOAc. When using GOAc, the amounts of α-terpinene and terpinolene were 35% and 5%, respectively, while NOAc as a substrate produced 34% and 24%, respectively (Fig. 1). We assume these products are formed primarily from cation **D**, which is slightly more stable than **C** (1.1 kcal/mol). Analysis of our HT-LMD simulation trajectories reveals that in the case of GOAc, acetic acid remains in the vicinity of carbon C3, as partial reattachment (i.e. electrostatic stabilization) to this position is necessary to form the reactive 2,3-cisoid cation. Hence, deprotonation at position C1, producing mostly α-terpinene, is a likely scenario. In the case of NOAc, acetic acid remains in the vicinity of C1, as the 2,3-cisoid cation is formed directly from C1-OAc cleavage. Here, deprotonation at either C1 or C7 is a possibility, yielding significant amounts of both α-terpinene and terpinolene. This might explain the elevated amounts of terpinolene when using NOAc. We measured the distances between C1 or C7 and the OAc oxygens and found that indeed, the acetic acid tends to remain near these carbons when NOAc turns into **C** or **D** (further information can be found in the SI, Fig. S7,a-c). We note that the difference between GOAc and NOAc can also be explained due to different chemical mechanisms, i.e. S$_N$1 and S$_N$2/S$_N$2', respectively.[2] This explanation is in line with the current simulation results, which suggest that GOAc clearly reacts in a stepwise fashion, whereas NOAc reacts in a more concerted fashion.

In conclusion, the current results suggest that the product distribution and the dependence on the initial leaving group is a combination of thermodynamic and kinetic factors. This suggests that if one starts with different initial substrates, one might bypass kinetic bottlenecks to reach more stable products. For example, one might be able to synthesize α-camphene by feeding the capsule with pinene, as we showed in this work.

Conclusion

In this work we presented a multiscale nano-reactor simulation approach. The nano-reactor simulation protocol consists of hybrid QM(DFT)/MM-based HT-LMD simulations. Using this approach we model the production of tail-to-head formation of monoterpenes inside a resorcin[4]arene-based capsule, and observe the chemical mechanisms as they occur inside the resorcinarene nano-environment. The HT-LMD simulations are able to generate all relevant carbocations that are precursors to the experimentally observed monoterpenes, as well as additional carbocations. We find that the best temperature for performing these types of QM/MM HT-LMD simulations of monoterpenes, are 900K – 1000K. Even short simulations, such as the ones performed in this work, can produce a variety of carbocations appearing inside the resorcinarene capsule. We combine this approach with extensive DFT calculations

of monoterpene stability, as well as detailed reaction mechanisms. Using this extensive computational platform, we explain two central questions related to terpene synthesis in nano-capsules: (1) What determines the observed product distribution inside capsule *I*? (2) What is the role of the substrate leaving group? The current results suggest that the product distribution is a result of a balance of thermodynamic and kinetic control: the experimentally observed products are low-energy species with low-energy carbocation precursors; however, the height of the free energy barriers dictates which pathways are accessible, and certain very low-energy monoterpenes are not observed. Specifically, most products formed experimentally are among the most stable known monoterpenes, suggesting thermodynamic control. However, some of the most stable monoterpenes were not observed, due to kinetic control. The effect of the initial leaving group (i.e. the difference in the product distribution between each initial substrate) is possibly due to a change from a stepwise to concerted mechanism. Based on this in silico platform, we suggested an initial substrate that was able to overcome the kinetic control and reach a thermodynamically more stable terpene. Additionally, we show that π-cation interactions with the capsule may direct the dynamic reaction cascades.

ASSOCIATED CONTENT

Supporting Information. Details of gas-phase calculations. Free energy for all monoterpenes. Comparison of gas-phase energies for all monoterpenes using DFT and high-level ab initio calculations. Details of the QM/MM HT-LMD simulations. Additional experimental data. Distance analyses from the HT-LMD trajectories. CHARMM topology and parameter files.

AUTHOR INFORMATION

Corresponding Author

* majort@biu.ac.il

Author Contributions

All authors have given approval to the final version of the manuscript.

REFERENCES

1. Zhang, Q.; Catti, L.; Pleiss, J.; Tiefenbacher, K., Terpene cyclizations inside a supramolecular catalyst: leaving-group-controlled product selectivity and mechanistic studies. *J. Am. Chem. Soc.* **2017,** *139* (33), 11482-11492.
2. Zhang, Q.; Tiefenbacher, K., Terpene cyclization catalysed inside a self-assembled cavity. *Nat. Chem.* **2015,** *7* (3), 197-202.
3. Firn, R., *Nature's chemicals: the natural products that shaped our world*. Oxford University Press on Demand: 2010.
4. Cane, D. E.; Ikeda, H., Exploration and mining of the bacterial terpenome. *Acc. Chem. Res.* **2011,** *45* (3), 463-472.
5. Breitmaier, E., *Terpenes: flavors, fragrances, pharmaca, pheromones*. John Wiley & Sons: 2006.
6. Gershenzon, J.; Dudareva, N., The function of terpene natural products in the natural world. *Nat. Chem. Biol.* **2007,** *3* (7), 408-414.
7. Christianson, D. W., Roots of Biosynthetic Diversity. *Science* **2007,** *316* (5821), 60-61.
8. Rastogi, N.; Abaul, J.; Goh, K. S.; Devallois, A.; Philogène, E.; Bourgeois, P., Antimycobacterial activity of chemically defined natural substances from the Caribbean flora in Guadeloupe. *FEMS Immunol. Med. Microbiol.* **1998,** *20* (4), 267-273.
9. Lunde, C. S.; Kubo, I., Effect of polygodial on the mitochondrial ATPase of Saccharomyces cerevisiae. *Antimicrob. Agents Chemother.* **2000,** *44* (7), 1943-1953.
10. Friedman, M.; Henika, P. R.; Mandrell, R. E., Bactericidal activities of plant essential oils and some of their isolated constituents against Campylobacter jejuni, Escherichia coli, Listeria monocytogenes, and Salmonella enterica. *J. Food Prot.* **2002,** *65* (10), 1545-1560.
11. Paddon, C. J.; Westfall, P. J.; Pitera, D. J.; Benjamin, K.; Fisher, K.; McPhee, D.; Leavell, M. D.; Tai, A.; Main, A.; Eng, D.; Polichuk, D. R.; Teoh, K. H.; Reed, D. W.; Treynor, T.; Lenihan, J.; Jiang, H.; Fleck, M.; Bajad, S.; Dang, G.; Dengrove, D.; Diola, D.; Dorin, G.; Ellens, K. W.; Fickes, S.; Galazzo, J.; Gaucher, S. P.; Geistlinger, T.; Henry, R.; Hepp, M.; Horning, T.; Iqbal, T.; Kizer, L.; Lieu, B.; Melis, D.; Moss, N.; Regentin, R.; Secrest, S.; Tsuruta, H.; Vazquez, R.; Westblade, L. F.; Xu, L.; Yu, M.; Zhang, Y.; Zhao, L.; Lievense, J.; Covello, P. S.; Keasling, J. D.; Reiling, K. K.; Renninger, N. S.; Newman, J. D., High-level semisynthetic production of the potent antimalarial artemisinin. *Nature* **2013,** *496*, 528-532.
12. Kingston, D. G., Recent advances in the chemistry of taxol. *J. Nat. Prod.* **2000,** *63* (5), 726-734.
13. Malik, S.; Cusidó, R. M.; Mirjalili, M. H.; Moyano, E.; Palazón, J.; Bonfill, M., Production of the anticancer drug taxol in Taxus baccata suspension cultures: a review. *Process Biochem.* **2011,** *46* (1), 23-34.
14. Lee, S.; Peterson, C. J.; Coats, J., Fumigation toxicity of monoterpenoids to several stored product insects. *J. Stored Prod. Res.* **2003,** *39* (1), 77-85.
15. Vourc'h, G.; De Garine-Wichatitsky, M.; Labbé, A.; Rosolowski, D.; Martin, J.-L.; Fritz, H., Monoterpene effect on feeding choice by deer. *J. Chem. Ecol.* **2002,** *28* (12), 2411-2427.
16. Dixit, M.; Weitman, M.; Gao, J.; Major, D. T., Chemical Control in the Battle against Fidelity in Promiscuous Natural Product Biosynthesis: The Case of Trichodiene Synthase. *ACS Catal.* **2017,** *7* (1), 812-818.
17. Christianson, D. W., Structural biology and chemistry of the terpenoid cyclases. *Chem. Rev.* **2006,** *106* (8), 3412-3442.
18. Weitman, M.; Major, D. T., Challenges posed to bornyl diphosphate synthase: diverging reaction mechanisms in monoterpenes. *J. Am. Chem. Soc.* **2010,** *132* (18), 6349-6360.
19. Major, D. T.; Weitman, M., Electrostatically Guided Dynamics-The Root of Fidelity in a Promiscuous Terpene Synthase? *J. Am. Chem. Soc.* **2012,** *134* (47), 19454-19462.
20. Freud, Y.; Ansbacher, T.; Major, D. T., Catalytic Control in the Facile Proton Transfer in Taxadiene Synthase. *ACS Catal.* **2017,** *7* (11), 7653-7657.
21. Ansbacher, T.; Freud, Y.; Major, D. T., Slow Starter Enzymes: Role of Active Site Architecture in the Catalytic Control in the Biosynthesis of Taxadiene by Taxadiene Synthase. *Biochemistry* **2018,** *57* (26), 3773-3779.
22. Christianson, D. W., Structural and Chemical Biology of Terpenoid Cyclases. *Chem. Rev.* **2017,** *117* (17), 11570-11648.
23. Tantillo, D. J., Importance of Inherent Substrate Reactivity in Enzyme - Promoted Carbocation Cyclization/Rearrangements. *Angew. Chem. Int. Ed.* **2017,** *56* (34), 10040-10045.
24. Wendt, K. U.; Schulz, G. E., Isoprenoid biosynthesis: manifold chemistry catalyzed by similar enzymes. *Structure* **1998,** *6* (2), 127-133.
25. Ruzicka, L., The isoprene rule and the biogenesis of terpenic compounds. *Experientia* **1953,** *9* (10), 357-367.
26. Croteau, R., Biosynthesis and catabolism of monoterpenoids. *Chem. Rev.* **1987,** *87* (5), 929-954.
27. Pronin, S. V.; Shenvi, R. A., Synthesis of highly strained terpenes by non-stop tail-to-head polycyclization. *Nat. Chem.* **2012,** *4* (11), 915-920.
28. Sarria, S.; Wong, B.; Martín, H. G.; Keasling, J. D.; Peralta-Yahya, P., Microbial synthesis of pinene. *ACS Synth. Biol.* **2014,** *3* (7), 466-475.
29. Major, D. T.; Freud, Y.; Weitman, M., Catalytic control in terpenoid cyclases: multiscale modeling of thermodynamic, kinetic, and dynamic effects. *Curr. Opin. Chem. Biol.* **2014,** *21*, 25-33.

30. Kobayashi, S.; Tsutsui, M.; Mukaiyama, T., Biogenetic-like cyclization of farnesol and nerolidol to bisabolene by the use of 2-fluorobenzothiazolium salt. *Chem. Lett.* **1977**, (10), 1169-1172.

31. Gutsche, C.; Maycock, J.; Chang, C., Acid-catalyzed cyclization of farnesol and nerolidol. *Tetrahedron* **1968**, *24* (2), 859-876.

32. Ohta, Y.; Hirose, Y., Electrophile induced cyclization of farnesol. *Chem. Lett.* **1972**, *1* (3), 263-266.

33. Sakane, S.; Fujiwara, J.; Maruoka, K.; Yamamoto, H., Chiral leaving group: asymmetric synthesis of limonene and bisabolene. *Tetrahedron* **1986**, *42* (8), 2193-2201.

34. Andersen, N.; Syrdal, D., Chemical simulation of the biogenesis of cedrene. *Tetrahedron Lett.* **1972**, *13* (24), 2455-2458.

35. Eschenmoser, A.; Arigoni, D., Revisited after 50 years: the 'stereochemical interpretation of the biogenetic isoprene rule for the triterpenes'. *Helv. Chim. Acta* **2005**, *88* (12), 3011-3050.

36. Stork, G.; Burgstahler, A., The stereochemistry of polyene cyclization. *J. Am. Chem. Soc.* **1955**, *77* (19), 5068-5077.

37. McCulley, C. H.; Geier, M. J.; Hudson, B. M.; Gagné, M. R.; Tantillo, D. J., Biomimetic Platinum-Promoted Polyene Polycyclizations: Influence of Alkene Substitution and Pre-cyclization Conformations. *J. Am. Chem. Soc.* **2017**, *139* (32), 11158-11164.

38. Johnson, W. S., Biomimetic polyene cyclizations: A review. *Bioorg. Chem.* **1976**, *5* (1), 51-98.

39. Corey, E.; Staas, D. D., Demonstration of a common concerted mechanistic pathway for the acid-catalyzed cyclization of 5, 6-unsaturated oxiranes in chemical and enzymatic systems. *J. Am. Chem. Soc.* **1998**, *120* (14), 3526-3527.

40. Yoder, R. A.; Johnston, J. N., A case study in biomimetic total synthesis: polyolefin carbocyclizations to terpenes and steroids. *Chem. Rev.* **2005**, *105* (12), 4730-4756.

41. Kronja, O.; Orlovic, M.; Humski, K.; Borcic, S., Lack of a secondary. beta.-deuterium kinetic isotope effect in the solvolysis of 2-chloro-3-hydrosqualene. A case of extended. pi.-participation and indication of concerted biomimetic polycyclization. *J. Am. Chem. Soc.* **1991**, *113* (6), 2306-2308.

42. Peralta-Yahya, P. P.; Zhang, F.; Del Cardayre, S. B.; Keasling, J. D., Microbial engineering for the production of advanced biofuels. *Nature* **2012**, *488* (7411), 320-328.

43. Mewalal, R.; Rai, D. K.; Kainer, D.; Chen, F.; Külheim, C.; Peter, G. F.; Tuskan, G. A., Plant-derived terpenes: A feedstock for specialty biofuels. *Trends Biotechnol.* **2017**, *35* (3), 227-240.

44. Phelan, R. M.; Sekurova, O. N.; Keasling, J. D.; Zotchev, S. B., Engineering terpene biosynthesis in Streptomyces for production of the advanced biofuel precursor bisabolene. *ACS Synth. Biol.* **2014**, *4* (4), 393-399.

45. Yang, J.; Li, Z.; Guo, L.; Du, J.; Bae, H.-J., Biosynthesis of β-caryophyllene, a novel terpene-based high-density biofuel precursor, using engineered Escherichia coli. *Renew. Energy* **2016**, *99*, 216-223.

46. Beller, H. R.; Lee, T. S.; Katz, L., Natural products as biofuels and bio-based chemicals: fatty acids and isoprenoids. *Nat. Prod. Rep.* **2015**, *32* (10), 1508-1526.

47. Zhang, F.; Rodriguez, S.; Keasling, J. D., Metabolic engineering of microbial pathways for advanced biofuels production. *Curr. Opin. Biotech.* **2011**, *22* (6), 775-783.

48. Peralta-Yahya, P. P.; Ouellet, M.; Chan, R.; Mukhopadhyay, A.; Keasling, J. D.; Lee, T. S., Identification and microbial production of a terpene-based advanced biofuel. *Nat. Commun.* **2011**, *2*, 483.

49. Leonard, E.; Ajikumar, P. K.; Thayer, K.; Xiao, W.-H.; Mo, J. D.; Tidor, B.; Stephanopoulos, G.; Prather, K. L., Combining metabolic and protein engineering of a terpenoid biosynthetic pathway for overproduction and selectivity control. *Proc. Natl. Acad. Sci. U. S. A.* **2010**, *107* (31), 13654-13659.

50. Martin, V. J.; Pitera, D. J.; Withers, S. T.; Newman, J. D.; Keasling, J. D., Engineering a mevalonate pathway in Escherichia coli for production of terpenoids. *Nat. Biotechnol.* **2003**, *21* (7), 796-802.

51. Leferink, N. G. H.; Jervis, A. J.; Zebec, Z.; Toogood, H. S.; Hay, S.; Takano, E.; Scrutton, N. S., A 'Plug and Play' Platform for the Production of Diverse Monoterpene Hydrocarbon Scaffolds in Escherichia coli. *ChemistrySelect* **2016**, *1*, 1893–1896.

52. Zebec, Z.; Wilkes, J.; Jervis, A. J.; Scrutton, N. S.; Takano, E.; Breitling, R., Towards synthesis of monoterpenes and derivatives using synthetic biology. *Curr. Opin. Chem. Biol.* **2016**, *34*, 37-43.

53. Karuppiah, V.; Ranaghan, K. E.; Leferink, N. G. H.; Johannissen, L. O.; Shanmugam, M.; Cheallaigh, A. N.; Bennett, N. J.; Kearsey, L. J.; Takano, E.; Gardiner, J. M.; Van der Kamp, M. W.; Hay, S.; Mulholland, A. J.; Leys, D.; Scrutton, N. S., Structural Basis of Catalysis in the Bacterial Monoterpene Synthases Linalool Synthase and 1,8-Cineole Synthase. *ACS Catal.* **2017**, *7*, 6268–6282.

54. Catti, L.; Zhang, Q.; Tiefenbacher, K., Advantages of Catalysis in Self‐Assembled Molecular Capsules. *Chem. Eur. J.* **2016**, *22* (27), 9060-9066.

55. Zhang, Q.; Catti, L.; Kaila, V. R.; Tiefenbacher, K., To catalyze or not to catalyze: elucidation of the subtle differences between the hexameric capsules of pyrogallolarene and resorcinarene. *Chem. Sci.* **2017**, *8* (2), 1653-1657.

56. MacGillivray, L. R.; Atwood, J. L., A chiral spherical molecular assembly held together by 60 hydrogen bonds. *Nature* **1997**, *389* (6650), 469-472.

57. Major, D. T., Complex terpenes in one pot. *Nat. Catal.* **2018**, *1* (8), 567-568.

58. Dougherty, D. A., The Cation-π Interaction. *Acc. Chem. Res.* **2012**, *46*, 885-893.

59. Sunner, J.; Nishizawa, K.; Kebarle, P., Ion-solvent molecule interactions in the gas phase. The potassium ion and benzene. *J. Phys. Chem.* **1981**, *85*, 1814–1820.

60. Diederich, F.; Dick, K., A new water-soluble macrocyclic host of the cyclophane type: Hostguest complexation with aromatic guests in aqueous solution and acceleration of the transport of arenes through an aqueous phase. *J. Am. Chem. Soc.* **1984**, *106*, 8024– 8036.

61. Burley, S. K.; Petsko, G. A., Amino-aromatic interactions in proteins. *FEBS Lett.* **1986**, *203*, 139-143.

62. Petti, M. A.; Shepodd, T. J.; Dougherty, D. A., Design and synthesis of a new class of hydrophobic binding sites. *Tetrahedron Lett.* **1986**, *27*, 807–810.

63. Ma, J. C.; Dougherty, D. A., The cation-π interaction. *Chem. Rev.* **1997**, *97*, 1303–1324.

64. Meot-Ner, M.; Deakyne, C. A., Unconventional ionic hydrogen bonds. 2. NH+···. *J. Am. Chem. Soc* **1985**, *107*, 474-479.

65. Wendt, K. U.; Poralla, K.; Schulz, G. E., Structure and Function of a Squalene Cyclase. *Science* **1997**, *277*, 1811–1815.

66. Salonen, L. M.; Ellermann, M.; Diederich, F., Aromatic rings in chemical and biological recognition: Energetics and structures. *Angew. Chem., Int. Ed.* **2011**, *50*, 4808–4842.

67. Pluth, M. D.; Bergman, R. G.; Raymond, K. N., Proton-mediated chemistry and catalysis in a self-assembled supramolecular host. *Acc. Chem. Res.* **2009**, *42* (10), 1650-1659.

68. Yoshizawa, M.; Fujita, M., Development of unique chemical phenomena within nanometer-sized, self-assembled coordination hosts. *Bull. Chem. Soc. Jpn.* **2010**, *83* (6), 609-618.

69. Ronson, T. K.; Zarra, S.; Black, S. P.; Nitschke, J. R., Metal–organic container molecules through subcomponent self-assembly. *Chem. Comm.* **2013**, *49* (25), 2476-2490.

70. Han, M.; Engelhard, D. M.; Clever, G. H., Self-assembled coordination cages based on banana-shaped ligands. *Chem. Soc. Rev.* **2014**, *43* (6), 1848-1860.

71. Zhang, G.; Mastalerz, M., Organic cage compounds–from shape-persistency to function. *Chem. Soc. Rev.* **2014**, *43* (6), 1934-1947.

72. Leenders, S. H.; Gramage-Doria, R.; De Bruin, B.; Reek, J. N., Transition metal catalysis in confined spaces. *Chem. Soc. Rev.* **2015**, *44* (2), 433-448.

73. Rebek Jr, J., Molecular behavior in small spaces. *Acc. Chem. Res.* **2009**, *42* (10), 1660-1668.

74. Ajami, D.; Rebek, J., More Chemistry in Small Spaces. *Acc. Chem. Res.* **2013**, *46* (4), 990-999.

75. Ballester, P.; Fujita, M.; Rebek, J., Molecular containers. *Chem. Soc. Rev.* **2015**, *44* (2), 392-393.

76. Jordan, J. H.; Gibb, B. C., Molecular containers assembled through the hydrophobic effect. *Chem. Soc. Rev.* **2015**, *44* (2), 547-585.

77. Wiester, M. J.; Ulmann, P. A.; Mirkin, C. A., Enzyme mimics based upon supramolecular coordination chemistry. *Angew. Chem. Int. Ed.* **2011**, *50* (1), 114-137.

78. Yoshizawa, M.; Klosterman, J. K.; Fujita, M., Functional molecular flasks: new properties and reactions within discrete, self‐assembled hosts. *Angew. Chem. Int. Ed.* **2009**, *48* (19), 3418-3438.

79. Marchetti, L.; Levine, M., Biomimetic catalysis. *ACS Catal.* **2011**, *1* (9), 1090-1118.

80. Brown, C. J.; Toste, F. D.; Bergman, R. G.; Raymond, K. N., Supramolecular catalysis in metal–ligand cluster hosts. *Chem. Rev.* **2015**, *115* (9), 3012-3035.

81. Zhang, Q.; Tiefenbacher, K., Hexameric resorcinarene capsule is a Brønsted acid: investigation and application to synthesis and catalysis. *J. Am. Chem. Soc.* **2013**, *135* (43), 16213-16219.

82.   Catti, L.; Tiefenbacher, K., Intramolecular hydroalkoxylation catalyzed inside a self-assembled cavity of an enzyme-like host structure. *Chem. Comm.* **2015,** *51* (5), 892-894.

83.   Köster, J. M.; Tiefenbacher, K., Elucidating the Importance of Hydrochloric Acid as a Cocatalyst for Resorcinarene‐Capsule‐Catalyzed Reactions. *ChemCatChem* **2018,** *10* (14), 2941-2944.

84.   Catti, L.; Zhang, Q.; Tiefenbacher, K., Self-Assembled Supramolecular Structures as Catalysts for Reactions Involving Cationic Transition States. *Synthesis* **2016,** *48* (03), 313-328.

85.   Bräuer, T. M.; Zhang, Q.; Tiefenbacher, K., Iminium Catalysis inside a Self‐Assembled Supramolecular Capsule: Modulation of Enantiomeric Excess. *Angew. Chem. Int. Ed.* **2016,** *55* (27), 7698-7701.

86.   Warshel, A.; Levitt, M., Theoretical studies of enzymic reactions: dielectric, electrostatic and steric stabilization of the carbonium ion in the reaction of lysozyme. *J. Mol. Biol.* **1976,** *103* (2), 227-249.

87.   Mohamadi, F.; Richards, N. G.; Guida, W. C.; Liskamp, R.; Lipton, M.; Caufield, C.; Chang, G.; Hendrickson, T.; Still, W. C., MacroModel—an integrated software system for modeling organic and bioorganic molecules using molecular mechanics. *J. Comput. Chem.* **1990,** *11* (4), 440-467.

88.   Gonzalez, C.; Schlegel, H. B., Reaction path following in mass-weighted internal coordinates. *J. Phys. Chem.* **1990,** *94* (14), 5523-5527.

89.   Vanommeslaeghe, K.; Hatcher, E.; Acharya, C.; Kundu, S.; Zhong, S.; Shim, J.; Darian, E.; Guvench, O.; Lopes, P.; Vorobyov, I., CHARMM general force field: A force field for drug‐like molecules compatible with the CHARMM all‐atom additive biological force fields. *J. Comput. Chem.* **2010,** *31* (4), 671-690.

90.   Harder, E.; Damm, W.; Maple, J.; Wu, C.; Reboul, M.; Xiang, J. Y.; Wang, L.; Lupyan, D.; Dahlgren, M. K.; Knight, J. L., OPLS3: a force field providing broad coverage of drug-like small molecules and proteins. *J. Chem. Theory Comput.* **2015,** *12* (1), 281-296.

91.   Frisch, M. J.; Trucks, G. W.; Schlegel, H. B.; Scuseria, G. E.; Robb, M. A.; Cheeseman, J. R.; Scalmani, G.; Barone, V.; Petersson, G. A.; Nakatsuji, H.; Li, X.; Caricato, M.; Marenich, A. V.; Bloino, J.; Janesko, B. G.; Gomperts, R.; Mennucci, B.; Hratchian, H. P.; Ortiz, J. V.; Izmaylov, A. F.; Sonnenberg, J. L.; Williams-Young, D.; Ding, F.; Lipparini, F.; Egidi, F.; Goings, J.; Peng, B.; Petrone, A.; Henderson, T.; Ranasinghe, D.; Zakrzewski, V. G.; J. Gao, N. R.; Zheng, G.; Liang, W.; Hada, M.; Ehara, M.; Toyota, K.; Fukuda, R.; Hasegawa, J.; Ishida, M.; Nakajima, T.; Honda, Y.; Kitao, O.; Nakai, H.; Vreven, T.; Throssell, K.; Montgomery, J. A.; Jr., J. E. P.; Ogliaro, F.; Bearpark, M. J.; Heyd, J. J.; Brothers, E. N.; Kudin, K. N.; Staroverov, V. N.; Keith, T. A.; Kobayashi, R.; Normand, J.; Raghavachari, K.; A. P. Rendell; J. C. Burant; S. S. Iyengar; J. Tomasi; M. Cossi; J. M. Millam; M. Klene; C. Adamo; R. Cammi; J. W. Ochterski; R. L. Martin; K. Morokuma; O. Farkas; J. B. Foresman; Fox, D. J. *Gaussian 16, revision A. 03*, 2016.

92.   Zhao, Y.; Truhlar, D. G., The M06 suite of density functionals for main group thermochemistry, thermochemical kinetics, noncovalent interactions, excited states, and transition elements: two new functionals and systematic testing of four M06-class functionals and 12 other functionals. *Theor. Chem. Acc.* **2008,** *120* (1-3), 215-241.

93.   Zhao, Y.; Truhlar, D. G., Density functionals with broad applicability in chemistry. *Acc. Chem. Res.* **2008,** *41* (2), 157-167.

94.   Hehre, W. J.; Ditchfield, R.; Pople, J. A., Self—consistent molecular orbital methods. XII. Further extensions of Gaussian—type basis sets for use in molecular orbital studies of organic molecules. *J. Chem. Phys.* **1972,** *56* (5), 2257-2261.

95.   Fukui, K., The path of chemical reactions-the IRC approach. *Acc. Chem. Res.* **1981,** *14* (12), 363-368.

96.   Scott, A. P.; Radom, L., Harmonic vibrational frequencies: an evaluation of Hartree− Fock, Møller− Plesset, quadratic configuration interaction, density functional theory, and semiempirical scale factors. *J. Phys. Chem.* **1996,** *100* (41), 16502-16513.

97.   Ghahremanpour, M. M.; Van Maaren, P. J.; Ditz, J. C.; Lindh, R.; Van der Spoel, D., Large-scale calculations of gas phase thermochemistry: Enthalpy of formation, standard entropy, and heat capacity. *J. Chem. Phys.* **2016,** *145* (11), 114305-12.

98.   Gutiérrez, I. S.; Lin, F.-Y.; Vanommeslaeghe, K.; Lemkul, J. A.; Armacost, K. A.; Brooks III, C. L.; MacKerell Jr, A. D., Parametrization of halogen bonds in the CHARMM general force field: Improved treatment of ligand–protein interactions. *Bioorg. Med. Chem.* **2016,** *24* (20), 4812-4825.

99.   Guvench, O.; Mallajosyula, S. S.; Raman, E. P.; Hatcher, E.; Vanommeslaeghe, K.; Foster, T. J.; Jamison, F. W.; MacKerell Jr, A. D., CHARMM additive all-atom force field for carbohydrate derivatives and its utility in polysaccharide and carbohydrate–protein modeling. *J. Chem. Theory Comput.* **2011,** *7* (10), 3162-3180.

100.   Klauda, J. B.; Venable, R. M.; Freites, J. A.; O'Connor, J. W.; Tobias, D. J.; Mondragon-Ramirez, C.; Vorobyov, I.; MacKerell Jr, A. D.; Pastor, R. W., Update of the CHARMM all-atom additive force field for lipids: validation on six lipid types. *J. Phys. Chem. B* **2010,** *114* (23), 7830-7843.

101.   Hart, K.; Foloppe, N.; Baker, C. M.; Denning, E. J.; Nilsson, L.; MacKerell Jr, A. D., Optimization of the CHARMM additive force field for DNA: Improved treatment of the BI/BII conformational equilibrium. *J. Chem. Theory Comput.* **2011,** *8* (1), 348-362.

102.   Best, R. B.; Zhu, X.; Shim, J.; Lopes, P. E.; Mittal, J.; Feig, M.; MacKerell Jr, A. D., Optimization of the additive CHARMM all-atom protein force field targeting improved sampling of the backbone φ, ψ and side-chain χ1 and χ2 dihedral angles. *J. Chem. Theory Comput.* **2012,** *8* (9), 3257-3273.

103.   Brooks, B. R.; Bruccoleri, R. E.; Olafson, B. D.; States, D. J.; Swaminathan, S. a.; Karplus, M., CHARMM: a program for macromolecular energy, minimization, and dynamics calculations. *J. Comput. Chem.* **1983,** *4* (2), 187-217.

104.   Brooks, B. R.; Brooks III, C. L.; Mackerell Jr, A. D.; Nilsson, L.; Petrella, R. J.; Roux, B.; Won, Y.; Archontis, G.; Bartels, C.; Boresch, S., CHARMM: the biomolecular simulation program. *J. Comput. Chem.* **2009,** *30* (10), 1545-1614.

105.   Van der Kamp, M. W.; Sirirak, J.; Żurek, J.; Allemann, R. K.; Mulholland, A. J., Conformational Change and Ligand Binding in the Aristolochene Synthase Catalytic Cycle. *Biochemistry* **2013,** *52*, 8094-8105.

106.   MacKerell Jr, A.; Bashford, D.; Bellott, M.; Dunbrack Jr, R.; Evanseck, J.; Field, M.; Fischer, S.; Gao, J.; Guo, H.; Ha, S.; Joseph-McCarthy, D.; Kuchnir, L.; Kuczera, K.; Lau, F. T. K.; Mattos, C.; Michnick, S.; Ngo, T.; Nguyen, D. T.; Prodhom, B.; Reiher, W. E.; Roux, B.; Schlenkrich, M.; Smith, J. C.; Stote, R.; Straub, J.; Watanabe, M.; Wirkiewicz-Kuczera, J.; Yin, D.; Karplus, M., All-Atom Empirical Potential for Molecular Modeling and Dynamics Studies of Proteins. *J. Phys. Chem. B* **1998,** *102* (18), 3586-3616.

107.   Allen, M. P.; Tildesley, D. J., *Computer simulation of liquids*. Oxford university press: 2017.

108.   Shao, Y. G., Z.; Epifanovsky, E.; Gilbert, A. T. B.; Wormit, M.; Kussmann, J.; Lange, A. W.; Behn, A.; Deng, J.; Feng, X.; Ghosh, D.; Goldey, M.; Horn, P. R.; Jacobson, L. D.; Kaliman, I.; Khaliullin, R. Z.; Kuś, T.; Landau, A.; Liu, J.; Proynov, E. I.; Rhee, Y. M.; Richard, R. M.; Rohrdanz, M. A.; Steele, R. P.; Sundstrom, E. J.; Woodcock, H. L.; Zimmerman, P. M.; Zuev, D.; Albrecht, B.; Alguire, E.; Austin, B.; Beran, G. J. O.; Bernard, Y. A.; Berquist, E.; Brandhorst, K.; Bravaya, K. B.; Brown, S. T.; Casanova, D.; Chang, C.-M.; Chen, Y.; Chien, S. H.; Closser, K. D.; Crittenden, D. L.; Diedenhofen, M.; DiStasio, R. A.; Do, H.; Dutoi, A. D.; Edgar, R. G.; Fatehi, S.; Fusti-Molnar, L.; Ghysels, A.; Golubeva-Zadorozhnaya, A.; Gomes, J.; Hanson-Heine, M. W. D.; Harbach, P. H. P.; Hauser, A. W.; Hohenstein, E. G.; Holden, Z.; Jagau, T.-C.; Ji, H.; Kaduk, B.; Khistyaev, K.; Kim, J.; Kim, J.; King, R. A.; Klunzinger, P.; Kosenkov, D.; Kowalczyk, T.; Krauter, C. M.; Lao, K. U.; Laurent, A. D.; Lawler, K. V; Levchenko, S. V; Lin, C. Y.; Liu, F.; Livshits, E.; Lochan, R. C.; Luenser, A.; Manohar, P.; Manzer, S. F.; Mao, S.-P.; Mardirossian, N.; Marenich, A. V; Maurer, S. A.; Mayhall, N. J.; Neuscamman, E.; Oana, C. M.; Olivares-Amaya, R.; O'Neill, D. P.; Parkhill, J. A.; Perrine, T. M.; Peverati, R.; Prociuk, A.; Rehn, D. R.; Rosta, E.; Russ, N. J.; Sharada, S. M.; Sharma, S.; Small, D. W.; Sodt, A.; Stein, T.; Stück, D.; Su, Y.-C.; Thom, A. J. W.; Tsuchimochi, T.; Vanovschi, V.; Vogt, L.; Vydrov, O.; Wang, T.; Watson, M. A.; Wenzel, J.; White, A.; Williams, C. F.; Yang, J.; Yeganeh, S.; Yost, S. R.; You, Z.-Q.; Zhang, I. Y.; Zhang, X.; Zhao, Y.; Brooks, B. R.; Chan, G. K. L.; Chipman, D. M.; Cramer, C. J.; Goddard, W. A.; Gordon, M. S.; Hehre, W. J.; Klamt, A.; Schaefer, H. F.; Schmidt, M. W.; Sherrill, C. D.; Truhlar, D. G.; Warshel, A.; Xu, X.; Aspuru-Guzik, A.; Baer, R.; Bell, A. T.; Besley, N. A.; Chai, J.-D.; Dreuw, A.; Dunietz, B. D.; Furlani, T. R.; Gwaltney, S. R.; Hsu, C.-P.; Jung, Y.; Kong, J.; Lambrecht, D. S.; Liang, W.; Ochsenfeld, C.; Rassolov, V. A.; Slipchenko, L. V; Subotnik, J. E.; Van Voorhis, T.; Herbert, J. M.; Krylov, A. I.; Gill, P. M. W.; Head-Gordon, M. , Advances in molecular quantum chemistry contained in the Q-Chem 4 program package. *Mol. Phys.* **2015,** *113* (2), 184-215.

109.   Wang, L.-P.; Titov, A.; McGibbon, R.; Liu, F.; Pande, V. S.; Martínez, T. J., Discovering chemistry with an ab initio nanoreactor. *Nat. Chem.* **2014,** *6* (12), 1044-1048.

110.   Zhang, Q.; Rinkel, J.; Goldfuss, B.; Dickschat, J. S.; Tiefenbacher, K., Sesquiterpene cyclizations catalysed inside the resorcinarene capsule and application in the short synthesis of isolongifolene and isolongifolenone. *Nat. Catal.* **2018,** *1* (8), 609-615.

111. Tian, B.; Poulter, C. D.; Jacobson, M. P., Defining the product chemical space of monoterpenoid synthases. *PLOS Comput. Biol.* **2016,** *12* (8), e1005053.

112. Montgomery Jr, J. A.; Frisch, M. J.; Ochterski, J. W.; Petersson, G. A., A complete basis set model chemistry. VI. Use of density functional geometries and frequencies. *J. Chem. Phys.* **1999,** *110* (6), 2822-2827.

113. Montgomery Jr, J. A.; Frisch, M. J.; Ochterski, J. W.; Petersson, G. A., A complete basis set model chemistry. VII. Use of the minimum population localization method. *J. Chem. Phys.* **2000,** *112* (15), 6532-6542.

114. Curtiss, L. A.; Redfern, P. C.; Raghavachari, K., Gaussian-4 theory. *J. Chem. Phys.* **2007,** *126*, 084108.

115. Major, D. T., Electrostatic control of chemistry in terpene cyclases. *ACS Catal.* **2017,** *7* (8), 5461-5465.

116. Das, S.; Dixit, M.; Major, D. T., First principles model calculations of the biosynthetic pathway in selinadiene synthase. *Bioorg. Med. Chem.* **2016,** *24* (20), 4867-4870.

117. Dixit, M.; Weitman, M.; Gao, J.; Major, D. T., Comment on "Substrate Folding Modes in Trichodiene Synthase: A Determinant of Chemo- and Stereoselectivity". *ACS Catal.* **2018,** *8* (2), 1371-1375.

118. Tantillo, D. J., Biosynthesis via carbocations: theoretical studies on terpene formation. *Nat. Prod. Rep.* **2011,** *28* (6), 1035-1053.

119. Hong, Y. J.; Tantillo, D. J., Biosynthetic consequences of multiple sequential post-transition-state bifurcations. *Nat. Chem.* **2014,** *6* (2), 104-111.

120. Hong, Y. J.; Tantillo, D. J., A potential energy surface bifurcation in terpene biosynthesis. *Nat. Chem.* **2009,** *1* (5), 384-389.

121. Hong, Y. J.; Tantillo, D. J., Quantum chemical dissection of the classic terpinyl/pinyl/bornyl/camphyl cation conundrum—the role of pyrophosphate in manipulating pathways to monoterpenes. *Org. Biomol. Chem.* **2010,** *8* (20), 4589-4600.

122. Croteau, R. B.; Shaskus, J. J.; Renstrom, B.; Felton, N. M.; Cane, D. E.; Saito, A.; Chang, C., Mechanism of the pyrophosphate migration in the enzymic cyclization of geranyl and linalyl pyrophosphates to (+)-and (-)-bornyl pyrophosphates. *Biochemistry* **1985,** *24* (25), 7077-7085.

123. Cane, D. E.; Saito, A.; Croteau, R.; Shaskus, J.; Felton, M., Enzymic cyclization of geranyl pyrophosphate to bornyl pyrophosphate. Role of the pyrophosphate moiety. *J. Am. Chem. Soc.* **1982,** *104* (21), 5831-5833.

124. Chayet, L.; Rojas, M. C.; Cori, O.; Bunton, C. A.; McKenzie, D. C., Complexes of bivalent cations with neryl and geranyl pyrophosphate: their role in terpene biosynthesis. *Bioorg. Chem.* **1984,** *12* (4), 329-338.

125. Bolhuis, P. G.; Chandler, D.; Dellago, C.; Geissler, P. L., Transition path sampling: Throwing ropes over rough mountain passes, in the dark. *Annu. Rev. Phys. Chem.* **2002,** *53* (1), 291-318.

TOC